ACS APPLIED MATERIALS & INTERFACES

Research Article

www.acsami.org

Enhanced Electrocatalytic Activity of MoS_x on TCNQ-Treated Electrode for Hydrogen Evolution Reaction

Yung-Huang Chang,*[,†,‡,§] Revannath D Nikam,[†,§,⊥,#] Cheng-Te Lin,[§,∥] Jing-Kai Huang,[§] Chien-Chih Tseng,[§] Chang-Lung Hsu,[§] Chia-Chin Cheng,[△] Ching-Yuan Su,[○] Lain-Jong Li,[□] and Daniel H.C. Chua*[,‡]

[‡]Department of Material Science and Engineering, National University of Singapore, Singapore 117574

[§]Institute of Atomic and Molecular Sciences, Academia Sinica. Taipei 10617, Taiwan

[⊥]Department of Chemistry, National Taiwan University, Taipei 106, Taiwan

[#]Nanoscience and Technology Program, Taiwan International Graduate Program, Institute of Physics, Academia Sinica, Taipei 115, Taiwan

[∥]Key Laboratory of Marine New Materials and Related Technology, Zhejiang Key Laboratory of Marine Materials and Protection Technology, Ningbo Institute of Material Technology & Engineering, Chinese Academy of Sciences, Ningbo 315201, China

[△]Department of Materials Science & Engineering, National Chiao Tung University, HsinChu 300, Taiwan

[○]Graduate Institute of Energy Engineering and Department of Mechanical Engineering, National Central University, Chung-Li 32001, Taiwan

[□]Physical Science and Engineering division, King Abdullah University of Science and Technology, Thuwal 23955-6900, Saudi Arabia

Supporting Information

ABSTRACT: Molybdenum sulfide has recently attracted much attention because of its low cost and excellent catalytical effects in the application of hydrogen evolution reaction (HER). To improve the HER efficiency, many researchers have extensively explored various avenues such as material modification, forming hybrid structures or modifying geometric morphology. In this work, we reported a significant enhancement in the electrocatalytic activity of the MoS_x via growing on Tetracyanoquinodimethane (TCNQ) treated carbon cloth, where the MoS_x was synthesized by thermolysis from the ammonium tetrathiomolybdate ($(NH_4)_2MoS_4$) precursor at 170 °C. The pyridinic N- and graphitic N-like species on the surface of carbon cloth arising from the TCNQ treatment facilitate the formation of Mo^{5+} and S_2^{2-} species in the MoS_x, especially with S_2^{2-} serving as an active site for HER. In addition, the smaller particle size of the MoS_x grown on TCNQ-treated carbon cloth reveals a high ratio of edge sites relative to basal plane sites, indicating the richer effective reaction sites and superior electrocatalytic characteristics. Hence, we reported a high hydrogen evolution rate for MoS_x on TCNQ-treated carbon cloth of 6408 mL g^{-1} cm^{-2} h^{-1} (286 mmol g^{-1} cm^{-2} h^{-1}) at an overpotential of V = 0.2 V. This study provides the fundamental concepts useful in the design and preparation of transition metal dichalcogenide catalysts, beneficial in the development in clean energy.

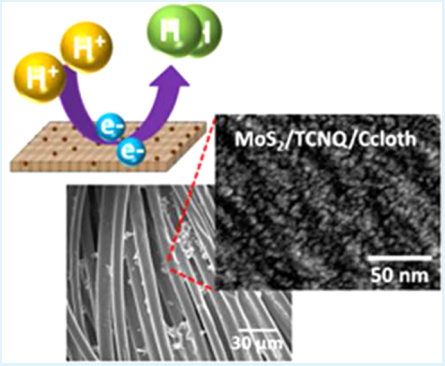

KEYWORDS: *hydrogen evolution reaction, electrocatalyst, molybdenium disulfide, transition metal dichalcogenides*

INTRODUCTION

Hydrogen energy is one of the most promising candidates for replacing petroleum fuels in the future if the process can occur without greenhouse gas byproducts. Two potential technologies, photo-[1−11] and electrocatalytic[12−28] techniques, have been developed for hydrogen evolution reaction for several decades. However, there still exist significant challenges to be overcome. For photocatalytic techniques, issues such as low production rate, low photon absorption capability and the separation issue for mixed H_2 and O_2 agents (especially for power catalysts) needs to be overcome. Despite the advantageous that photoelectrochemical (PEC) cells not having the separation issue, the current density generated by the PEC cell is still about 3 orders of magnitude lower than the electrocatalytic water splitting.[29] Hence, one focus of research in hydrogen evolution reaction (HER) is based on electrocatalytic processes that attract much interest worldwide.[12−28] In addition, the highly efficient platinum electrode serving as an electrocatalyst further impedes the adoption of this application in the industry because of its high cost and rareness.[30] As a result, there is an

Received: June 20, 2014
Accepted: September 30, 2014
Published: September 30, 2014

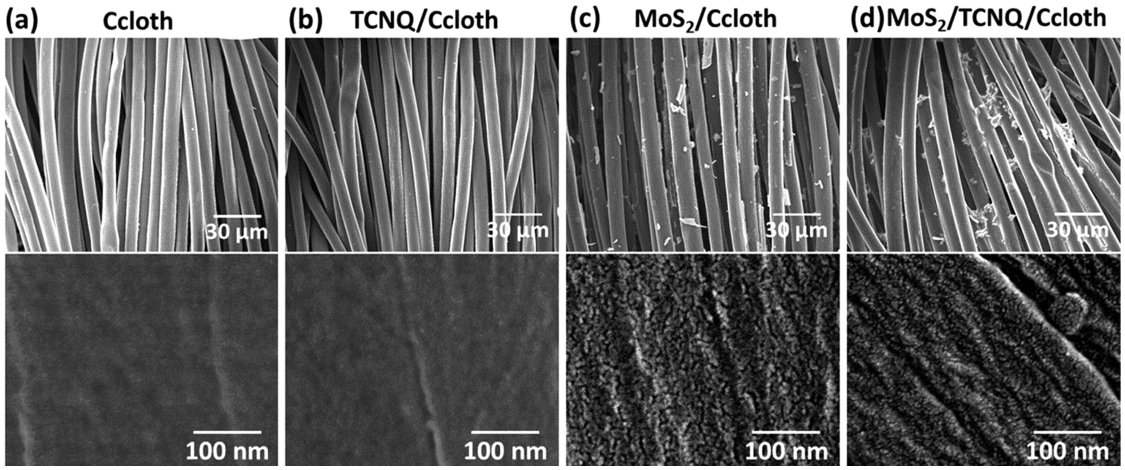

Figure 1. SEM images showing the morphology of (a) pristine carbon cloth, (b) decorated carbon cloth after a TCNQ process, (c) the MoS_x catalysts grown on pristine carbon cloth, and (d) the MoS_x catalysts grown on TCNQ-treated carbon cloth.

intensive search for an inexpensive and earth abundant substitute. Recently, molybdenum disulfide (MoS_2) shown low cost, chemical stability and high efficiency in HER would be a promising candidate for the development of hydrogen energy devices.[31,32] To further enhance its HER, there are many reports ranging from the modification of material properties,[33−36] morphologies,[37,38] and/or hybrid structures.[39−41] Amorphous MoS_2 grown from $(NH_4)_2MoS_4$ precursor at low temperature have shown an great enhancement in current density resulting from the enlarged amount of S_2^{2-} serving as a reaction site.[12,31] In addition to the characteristic modification in materials, the high surface curvature of a double-gyroid MoS_2 architecture exposes a lot of edge sites on the surface, leading to outstanding electrochemical activity.[37] Besides, highly conductive reduced graphene oxide (RGO) has been reported to be used successfully as a template to host MoS_2 catalysts thus further enhancing the conductance of the catalysts.[39,40] Recently, in order to increase the number of reaction sites, three-dimensional MoS_x catalysts grown on graphene-coated Ni foam or on commercial sponges have been successfully prepared.[42,43]

In this article, we provide a simple way to enhance the electrocatalytic activity, which is based on characteristic modification and morphological improvement simultaneously. In this study, MoS_x catalysts grown on TCNQ-treated carbon cloth from $(NH_4)_2MoS_4$ precursor by using a one-step and scalable thermolysis process have been prepared. According to the results, the pyridinic N- and graphitic N-like species on the surface of carbon cloth after the TCNQ process are proposed to be the factor to enlarge the amount of S_2^{2-} species and narrow the MoS_x particle size, resulting in the improvement of electrocatalytic activity.

EXPERIMENTAL SECTION

The commercial carbon cloth (W0S1002 from CeTech) was used as the conducting substrate to load the precursors for MoS_x synthesis. First, tetracyanoquinodimethane (TCNQ, formula $(NC)_2CC_6H_4C(CN)_2$) powder and carbon cloth were introduced into a sealed chamber contain 1 mTorr presuure and then the same environment was maintained at 1000 °C for 30 min to modify the surface of carbon cloth. After that the TCNQ-treated carbon cloth was immersed into ammonium thiomolybdate solution (5 wt % of $(NH_4)_2MoS_4$ in dimethylformamide) for precursor coating, and then the $(NH_4)_2MoS_4$/TCNQ/carbon cloth samples were dried on a hot plate at 100 °C for 5 min. Afterward the $(NH_4)_2MoS_4$/TCNQ/carbon cloth samples were fed into a hot-wall tube furnace for thermolysis and the environment was kept at 500 Torr with the gas mixture of H_2 and Ar (20 and 80 sccm, respectively). The MoS_x grown on TCNQ-modified carbon cloth was formed after subsequent annealing at 170 °C for 1 h. Besides, the growth method for MoS_x catalysts on pristine carbon cloth was in the same way except the TCNQ process.

Raman spectra were used to identify the composition of the samples and the spectra were collected by a NT-MDT confocal Raman microscope and the exciting laser wavelength and laser spot size are 473 and ∼500 nm, respectively. The data were recorded for 10 s for each sample. Si peak at 520 cm^{-1} was used as a reference for calibration in Raman characterization. Chemical configurations were determined by X-ray photoelectron spectroscope (XPS, Phi V5000). XPS measurements were performed with an Mg Kα X-ray source on the samples. The energy calibrations were made against the C 1s peak to eliminate the charging of the sample during analysis. Fourier transform infrared spectroscopy (FTIR) characterization was performed at room temperature in ambient with a FTIR spectrometer (Frontier Optica). Surface morphology of samples was examined with a field-emission scanning electron microscope (FESEM, JSM-6500F) and a transmission electron microscope (TEM, JEM-2100F). Electrochemical polarization curves were recorded by AUTOLAB pontentiostat (PGSTAT 302N) with a scan rate of 5 mV/s in 0.5 M H_2SO_4 electrolyte. A three-electrode configuration was adopted for polarization and electrolysis measurements using an Ag/AgCl (3.0 mol/kg KCl) electrode as the reference electrode while a graphite rod was used as the counter electrode and the MoS_2 samples as the working electrode. The bias voltages applied were then presented with the correction to the reversible hydrogen electrode (RHE).

RESULTS AND DISCUSSION

The scanning electron microscopy (SEM) images a and b in Figure 1 show the morphology of the pristine and decorated carbon cloth after a TCNQ process, respectively. Images c and d in Figure 1 present the SEM images of the MoS_x catalysts on the pristine and TCNQ-treated carbon cloth after the thermolysis process at 170 °C, respectively. The surface of pristine and TCNQ-treated carbon cloth is fairly smooth, and the differences are not visually visible. However, after MoS_x coating, the surface of pristine and TCNQ-treated carbon cloth is relatively rough. The morphology of the MoS_x on pristine carbon cloth is large concentrations of nanosized particles tightly clustered together. The nanosized particles have been observed to have an average diameter of ∼5 nm for the MoS_x

on TCNQ-treated specimens, as shown in Figure S1 in the Supporting Information. As such, the particle size for MoS_x grown on TCNQ-treated carbon cloth is smaller than those on pristine carbon cloth.

Figure 2 shows the Raman spectra of the MoS_x grown on pristine and TCNQ-treated carbon cloth. The characteristic

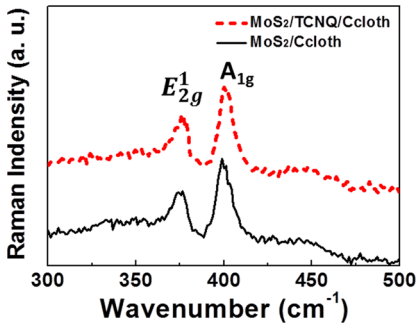

Figure 2. Raman spectra of the MoS_x grown on pristine carbon cloth and TCNQ-treated carbon cloth at 170 °C.

peaks of MoS_x on pristine carbon cloth are E^1_{2g} at 374.0 cm^{-1} and A_{1g} at 400.3 cm^{-1}.[44] For MoS_x on TCNQ-treated carbon cloth, the characteristic peaks including E^1_{2g} at 374.0 cm^{-1} and A_{1g} at 401.3 cm^{-1} are observed. The difference between A_{1g} and E^1_{2g} is >26.3 cm^{-1}, indicating that the bulk property is revealed rather than layered structures. Compared with CVD MoS_2 (403.8 and 385.8 cm^{-1}),[45] the red shift phenomenon for Raman spectrum are revealed and may be attributed to the effects of defects or carrier concentration[46,47] on phonon vibration resulting from amorphous nanoparticle structures. However, no characteristic peaks are found from X-ray diffraction (XRD) profiles in Figure S2 in the Supporting Information, indicating that the MoS_x formed at such a low temperature is an amorphous structure.[12,31]

Figure 3 shows the detailed X-ray photoemission spectroscopy (XPS) examinations of the C and N binding energies for pristine and TCNQ-treated carbon cloth. For pristine carbon cloth, the high-resolution C 1s peak can be fitted into a main peak at 284.5 eV and a slight peak at 286.1 eV, corresponding to the sp^2 carbon and other oxygenated carbons such as C−O, respectively, whereas the N 1s peak was not found in the spectrum.[48,49] However, the TCNQ-treated carbon cloth exhibits a broader C 1s peak, which could be fitted into a major peak at 284.5 eV and two minor peaks at 285.8 and 287.4 eV. The major peak at 284.5 eV is attributed to a sp^2 carbon structure, and the minor peak at 285.8 eV could be associated with C═N bonding.[48,49] Besides, either the quinone group (C═O) or C≡N bonding is suggested to contribute to the minor peak at 287.4 eV.[50,51] Meanwhile, the N 1s peaks were investigated with well fitting, including two major peaks at 398.2 and 400.9 eV and a minor peak at 403.4 eV. For N 1s peaks located at 398.2 and 400.9 eV, the pyridinic N- and graphitic N-like species are proposed to be the bonding structures, respectively, consistent with the observation at C 1s peak.[52−54] In addition, the pyridine N-oxide structure could be confirmed to be responsible for the minor peak at 403.4 eV.[52] To further confirm the nitrogen-related species, the FTIR spectra of bare and TCNQ-treated carbon cloth are recorded in Figure S3 in the Supporting Information. The broad peaks at 800−1300 cm^{-1} could be resulted from C−N and C−O bonding.[55] The O−H groups may be resulted in a small peak at ∼1410 cm^{-1}.[55] The broad peak at ∼1700 cm^{-1} could be assigned to C═N and C═O groups.[49] Furthermore, no nitrogen-related peaks are examined in bare carbon cloth. Hence, the FTIR results are absolutely in agreement with the examinations in XPS. Besides, no typical TCNQ characteristic peaks at 1210, 1450, and 2230 cm^{-1} [56] are observed in Raman spectrum after a TCNQ process shown in Figure S4 in the Supporting Information, indicating decomposition and re-structuring for C and N elements. Therefore, the decoration on the surface of carbon cloth using the pyridinic N- and graphitic N-like species via a TCNQ- process has been demonstrated from XPS and FTIR analyses.

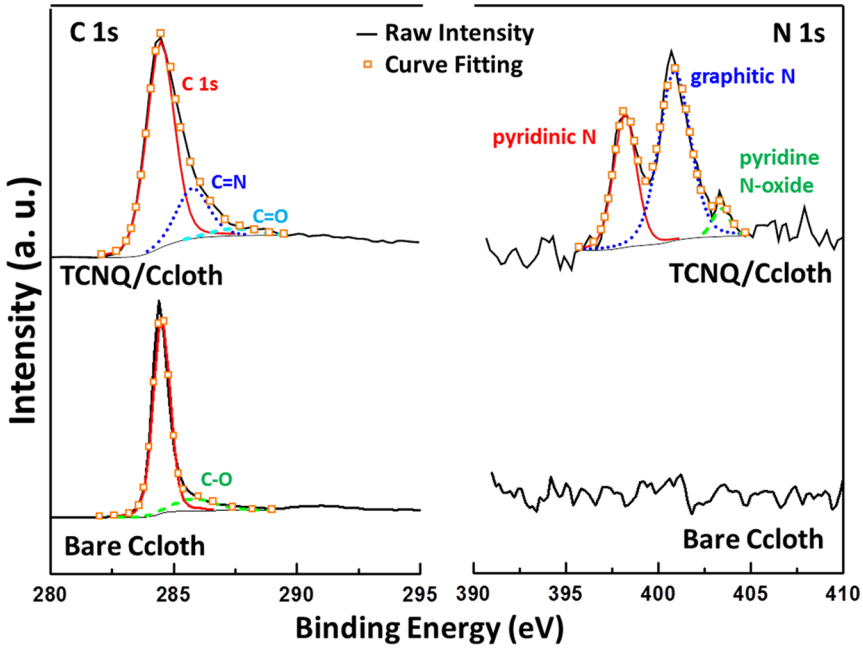

Figure 3. XPS spectra of C 1s peak and N 1s peak prepared on pristine carbon cloth and TCNQ-treated carbon cloth.

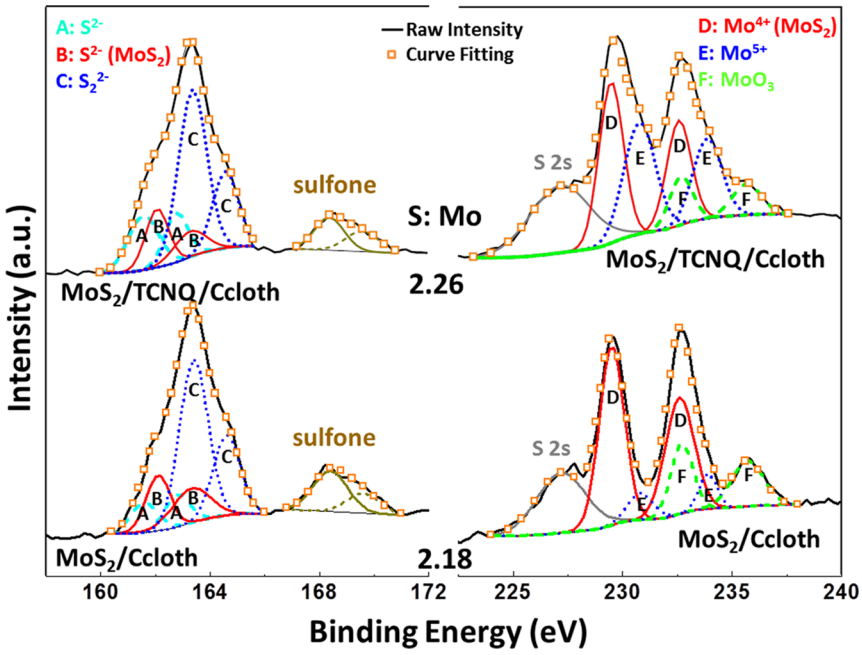

Figure 4. XPS spectra of S $2p_{3/2-1/2}$ peaks and Mo $3d_{5/2-3/2}$ peaks for the MoS_x catalysts grown on pristine and TCNQ-treated carbon cloth. Doublet B peaks correspond to the S^{2-} as in MoS_2 (162.1−163.3 eV) and the two partially overlapping doublets attributed to S^{2-} on the low energy side (shown as A; 161.6−162.8 eV) and to S_2^{2-} pairs on the high energy side (shown as C; 163.4−164.6 eV). Here the peak **A** and peak C is relative to the mixed environment as in MoS_3. Doublet D is for Mo^{4+} (229.5−232.6 eV) as in MoS_2, doublet E for Mo^{5+} (230.8−233.9 eV) in a mixed environment as in MoS_3, and F for Mo^{6+} (232.7−235.7 eV) at oxygen-rich surrounding for molybdenum atoms as in MoO_3.

To understand the differences between the MoS_x catalysts grown on pristine and TCNQ-treated carbon cloth, the detailed XPS measurements for Mo and S binding energy were used to characterize the chemical bonding structures, as shown in Figure 4. Only MoS_2-related elements are found in the XPS survey spectra in Figure S5 in the Supporting Information, indicating well-coating for the MoS_x material. For the MoS_x catalysts grown on pristine and TCNQ-treated carbon cloth, the Mo $3d_{5/2-3/2}$ can be fitted into several doublets, D for Mo^{4+} (229.5−232.6 eV) as in MoS_2, E for Mo^{5+} (230.8−233.9 eV) in a mixed environment as in MoS_3, and F for Mo^{6+} (232.7−235.7 eV) at oxygen-rich surrounding for molybdenum atoms as in MoO_3.[12,57−59] The S 2s peak at 227.2 eV belonging to MoS_2 is found in the spectra.[57] Because of the unstability for $(NH_4)_2MoS_4$ during the impregnation process, MoO_3 structure is formed easily at low temperature, whereas it is inexistent over a temperature of 300 °C (see the Supporting Information, Figure S6). Furthermore, the amount of Mo^{5+} species presented in the MoS_x catalysts is enhanced after the TCNQ process, as shown in Figure 4. In other words, the TCNQ-processed products, pyridinic N- and graphitic N-like species, violently influence the component in the MoS_x catalysts, especially the increase in Mo^{5+} species. This observation is also confirmed by the S $2p_{3/2-1/2}$ spectra shown in Figure 4, where B peaks correspond to the S^{2-} in MoS_2 (162.1−163.3 eV), and the two partially overlapping doublets attribute to S^{2-} on the low energy side (shown as A; 161.6−162.8 eV) and to S_2^{2-} pairs on the high energy side (shown as C; 163.4−164.6 eV).[12,59,60] An extra pair of doublet corresponding to sulfone was also found at 168.4 and 169.6 eV.[61] Here the peak A and peak C is relative to the mixed environment as in MoS_3. These two peaks existing at low temperature are almost disappeared at high temperature for crystallization in MoS_2 consistent with the report by Chen et al. (see the Supporting Information, Figure S6).[12] In general, the presence of Mo^{5+} species accompany the emergence of S_2^{2-} related species. Hence, in the Mo^{5+} rich environment, the percentage of S_2^{2-} related species was also increased from 76.0% up to 81.4% after the TCNQ process. In addition, the ratio of sulfur to molybdenum is 2.26 for MoS_x on TCNQ-treated carbon cloth, which is better than 2.18 for MoS_x on pristine carbon cloth. This result could be attributed to the suppression of reduction reaction of MoS_3 to MoS_2 through the pyridinic N- and graphitic N-like species on the carbon cloth.[45] As a result, the amount of Mo^{5+} and S_2^{2-} in MoS_x was promoted via the surface modification from the TCNQ process.

Figure 5a shows the polarization curves of the MoS_x grown on pristine and TCNQ-treated carbon cloth, where the current density is normalized by the projected area (or geometrical area) of the carbon cloth. Before the measurements on MoS_x, the pristine and TCNQ-treated carbon cloth was examined to make sure that these substrates do not contribute to the HER. The current density for the MoS_x on TCNQ-treated carbon cloth is about 209 mA/cm^2 (at −300 mV vs RHE), which is much better than 142 mA/cm^2 for the MoS_x on pristine carbon cloth. In previous studies and literatures,[12,20,31] the amorphous MoS_2, possessing both S^{2-} and S_2^{2-}, exhibits more excellent electrocatalytic behavior in hydrogen generation than crystalline MoS_2, possessing S^{2-} only. Hence, these unsaturated sulfur atoms in these materials such as bridging S_2^{2-} could be related to the HER activity.[31,39] Besides, the loading amount of MoS_x on pristine and TCNQ-treated carbon cloth is 3.39 and 3.41 mg/cm^2, respectively, so that the similar loading mass for MoS_x is not the main factor to affect the difference in the electrocatalytic current density. Therefore, the S_2^{2-} rich MoS_x material promoting via the TCNQ process reveals outstanding electrocatalytic activity in HER rather than that without the treatment. In addition, Figure 5b displays the Tafel plot and the fitting curves for these MoS_x grown on pristine and TCNQ-

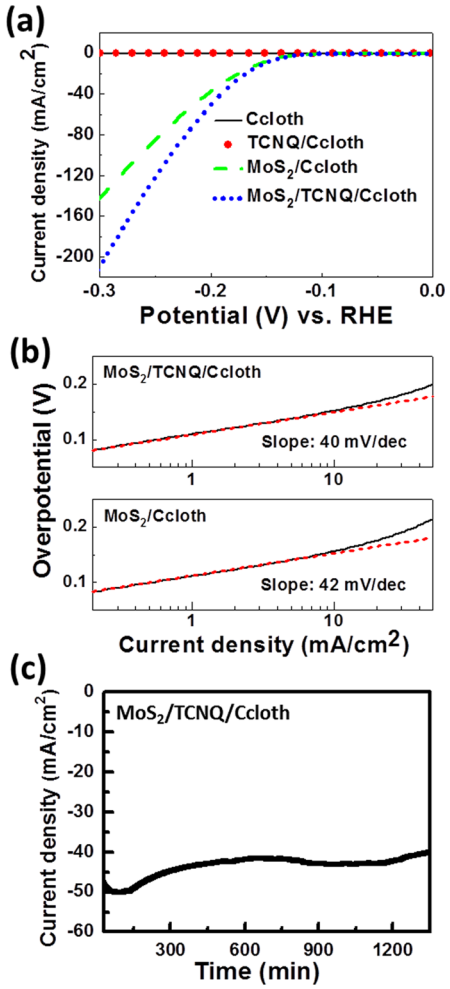

Figure 5. (a) Polarization curves and (b) Tafel plots for the MoS_x catalysts grown on pristine and TCNQ-treated carbon cloth at a scan rate of 5 mV/s in 0.5 M H_2SO_4 electrolyte. (c) Durability test of the MoS_x on TCNQ-treated carbon cloth with applied voltage of −200 mV vs RHE for 20 h.

treated carbon cloth. The Tafel equation $\eta = a + b \log j$ was used to obtain Tafel slope b, which is relative to the inherent property of the catalyst and is determined by the rate-limiting step of the HER. The Tafel slopes of 42 and 40 mV/decade were observed for MoS_x on pristine and TCNQ-treated carbon cloth, respectively. Hence, the two-step HER reaction mechanism is suggested to be the Volmer_Heyrovsky reaction, indicating the discharge step first followed by the electrochemical desorption step.[39] The durability of the MoS_x catalysts is also tested for more than 20 h, as shown in Figure 5c. The MoS_2 catalysts on TCNQ-treated carbon cloth show relatively stable current density after 300 min due to MoS_2 catalyst exfoliation from violent bubbles in the initial stage. The current density of the MoS_x is kept almost constant throughout the testing period in ambient environment. As a result, the MoS_x can serve as an electrocatalyst in acidic solution for a long working time.

Figure 6a shows the hydrogen gas evolution rate for the MoS_x on pristine carbon cloth, TCNQ-treated carbon cloth and graphene-protected Ni foam (previous study),[38] which is normalized by the weight of the catalyst and the projected area of the substrate. The highest hydrogen production rate we have achieved is around 6408 mL g^{-1} cm^{-2} h^{-1} (286 mmol g^{-1} cm^{-2} h^{-1}) at an overpotential V = 0.2 V for the MoS_x on TCNQ-treated carbon cloth. Note that the current density for the sample operated at 0.2 V is around 51 mA/cm^2. In addition to the S_2^{2-}-rich characteristic, the another advantage of using the TCNQ-treated carbon cloth as an electrode is that the particle size for the MoS_x is smaller than the other electrodes, as shown in Figure 6b. The smaller particle size owning high surface curvature exhibits abundant edge sites along surface morphology, resulting in excellent electrocatalytic activity for hydrogen evolution.[37] As a result, the superior performance for the MoS_x on TCNQ-treated carbon cloth is attributed to the S_2^{2-} rich characteristic as well as the abundant edge sites on the surface. For comparison with other reports, we have tabulated the HER Tafel slope and current density obtained from this work and those available in literature (see the Supporting Information, Table S1).

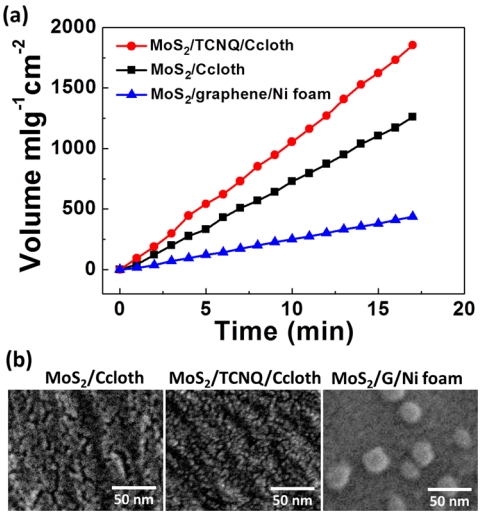

Figure 6. (a) Measured hydrogen gas evolution rate for the MoS_x on pristine carbon cloth, TCNQ-treated carbon cloth and graphene-protected Ni foam normalized by the weight of the catalysts and the projected area of the substrate. (b) SEM images showing the different particle sizes for the MoS_x catalysts grown on pristine carbon cloth, TCNQ-treated carbon cloth, and graphene-protected Ni foam.

CONCLUSIONS

We have performed a simple and scalable thermolysis process to prepare electroactive MoS_x catalysts on pristine and TCNQ-treated carbon cloth in the application of HER. The MoS_x on the TCNQ-treated carbon cloth shows more excellent current density of 51 mA/cm^2 at an overpotential of V = 0.2 V than 38 mA/cm^2 on the pristine one. The superior electrocatalytic capability for the MoS_x on TCNQ-treated carbon cloth could be attributed to the effect of the pyridinic N- and graphitic N-like species, arising from the TCNQ treatment. The pyridinic N- and graphitic N-like species on carbon cloth enhance the amount of Mo^{5+} and S_2^{2-} in the MoS_x, further reducing the size of the MoS_x particles, hence indicating that more active sites are provided for HER. A high hydrogen evolution rate up to 6408 mL g^{-1} cm^{-2} h^{-1} (286 mmol g^{-1} cm^{-2} h^{-1}) for MoS_x on TCNQ-modified carbon cloth was obtained. In addition, the MoS_x catalysts display outstanding stability and durability when they are operated in acidic electrolytes. This work provides a new strategy in the modification of intrinsic materials to form more electroactive electrodes for the future design in green energy.

■ ASSOCIATED CONTENT

Supporting Information

TEM image of MoS_x nanoparticles prepared on TCNQ-treated carbon cloth. XRD spectrum of the MoS_x on carbon cloth. FTIR and Raman spectra of bare and TCNQ-decorated carbon cloth. XPS survey spectra for MoS_x grown on pristine and TCNQ-treated carbon cloth. XPS spectra for MoS_x catalysts grown on carbon cloth at 120, 170, and 300 °C. Comparison of loading mass, Tafel slope, HER current density, and device structures for various MoS_2 electrocatalytic systems. This material is available free of charge via the Internet at http://pubs.acs.org/.

■ AUTHOR INFORMATION

Corresponding Authors

*E-mail: msecy@nus.edu.sg.

*E-mail: danielchua@nus.edu.sg.

Author Contributions

†Y.-H.C. and R.D.N. contributed equally.

Notes

The authors declare no competing financial interest.

■ ACKNOWLEDGMENTS

This research was supported by National Research Foundation, Prime Minister's Office, Singapore, under its Competitive Research Programme (CRP Award No. NRF-CRP 10-2012-6), Academia Sinica (IAMS and Nano program), and National Science Council Taiwan (NSC-99−2112-M-001−021-MY3). J.L. thanks the support from AOARD-134137.

■ REFERENCES

(1) Chuangchote, S.; Jitputti, J.; Sagawa, T.; Yoshikawa, S. Photocatalytic Activity for Hydrogen Evolution of Electrospun TiO_2 Nanofibers. *ACS Appl. Mater. Interfaces* **2009**, *1*, 1140−1143.

(2) Zhu, M.; Li, Z.; Xiao, B.; Lu, Y.; Du, Y.; Yang, P.; Wang, X. Surfactant Assistance in Improvement of Photocatalytic Fydrogen Production with the Porphyrin Noncovalently Functionalized Graphene Nanocomposite. *ACS Appl. Mater. Interfaces* **2013**, *5*, 1732−1740.

(3) Zhang, J.; Wang, Y.; Zhang, J.; Lin, Z.; Huang, F.; Yu, J. Enhanced Photocatalytic Hydrogen Production Activities of Au-Loaded ZnS Flowers. *ACS Appl. Mater. Interfaces* **2013**, *5*, 1031−1037.

(4) Zhang, J.; Wang, Y.; Jin, J.; Zhang, J.; Lin, Z.; Huang, F.; Yu, J. Efficient Visible-Light Photocatalytic Hydrogen Evolution and Enhanced Photostability of Core/shell CdS/g$^-$$C_3N_4$ Nanowires. *ACS Appl. Mater. Interfaces* **2013**, *5*, 10317−10324.

(5) Kargar, A.; Jing, Y.; Kim, S. J.; Riley, C. T.; Pan, X.; Wang, D. ZnO/CuO Heterojunction Branched Nanowires for Photoelectrochemical Hydrogen Generation. *ACS Nano* **2013**, *7*, 11112−11120.

(6) Maeda, K. Rhodium-Doped Barium Titanate Perovskite as a Stable P$^-$Type Semiconductor Photocatalyst for Hydrogen Evolution under Visible Light. *ACS Appl. Mater. Interfaces* **2014**, *6*, 2167−2173.

(7) Chiang, C.-Y.; Epstein, J.; Brown, A.; Munday, J. N.; Culver, J. N.; Ehrman, S. Biological Templates for Antireflective Current Collectors for Photoelectrochemical Cell Applications. *Nano Lett.* **2012**, *12*, 6005−6011.

(8) Frame, F. A.; Osterloh, F. E. CdSe-MoS_2: A Quantum Size-Confined Photocatalyst for Hydrogen Evolution from Water under Visible Light. *J. Phys. Chem. C* **2010**, *114*, 10628−10633.

(9) Tang, M. L.; Grauer, D. C.; Lassalle-Kaiser, B.; Yachandra, V. K.; Amirav, L.; Long, J. R.; Yano, J.; Alivisatos, A. P. Structural and Electronic Study of an Amorphous MoS_3 Hydrogen-Generation Catalyst on a Quantum-Controlled Photosensitizer. *Angew. Chem., Int. Ed.* **2011**, *123*, 10385−10389.

(10) Xiang, Q.; Yu, J.; Jaroniec, M. Synergetic Effect of MoS_2 and Graphene as Cocatalysts for Enhanced Photocatalytic H_2 Production Activity of TiO_2 Nanoparticles. *J. Am. Chem. Soc.* **2012**, *134*, 6575−6578.

(11) Zhang, J.; Yu, J.; Jaroniec, M.; Gong, J. R. Noble Metal-Free Reduced Graphene Oxide-$Zn_xCd_{1-x}S$ Nanocomposite with Enhanced Solar Photocatalytic H_2-Production Performance. *Nano Lett.* **2012**, *12*, 4584−4589.

(12) Chen, T.-Y.; Chang, Y.-H.; Hsu, C.-L.; Wei, K.-H.; Chiang, C.-Y.; Li, L.-J. Comparative Study on MoS_2 and WS_2 for Electrocatalytic Water Splitting. *Int. J. Hydrogen Energy* **2013**, *38*, 12302−12309.

(13) Zheng, Y.; Jiao, Y.; Zhu, Y.; Li, L. H.; Han, Y.; Chen, Y.; Du, A.; Jaroniec, M.; Qiao, S. Z. Hydrogen Evolution by a Metal-Free Electrocatalyst. *Nat. Commun.* **2014**, *5*, 3783−1−8.

(14) Yu, Y.; Huang, S.-Y.; Li, Y.; Steinmann, S. N.; Yang, W.; Cao, L. Layer-Dependent Electrocatalysis of MoS_2 for Hydrogen Evolution. *Nano Lett.* **2014**, *14*, 553−558.

(15) Huang, Z.; Wang, C.; Chen, Z.; Meng, H.; Lv, C.; Chen, Z.; Han, R.; Zhang, C. Tungsten Sulfide Enhancing Solar-Driven Hydrogen Production from Silicon Nanowires. *ACS Appl. Mater. Interfaces* **2014**, DOI: 10.1021/am501940x.

(16) Youn, D. H.; Han, S.; Kim, J. Y.; Kim, J. Y.; Park, H.; Choi, S. H.; Lee, J. S. Highly Active and Stable Hydrogen Evolution Electrocatalysts Based on Molybdenum Compounds on Carbon Nanotube−Graphene Hybrid Support. *ACS Nano* **2014**, *8*, 5164−5173.

(17) Yan, Y.; Ge, X.; Liu, Z.; Wang, J.-Y.; Lee, J.-M.; Wang, X. Facile Synthesis of Low Crystalline MoS_2 Nanosheet-Coated CNTs for Enhanced Hydrogen Evolution Reaction. *Nanoscale* **2013**, *5*, 7768−7771.

(18) Kong, D.; Wang, H.; Lu, Z.; Cui, Y. $CoSe_2$ Nanoparticles Grown on Carbon Fiber Paper: An Efficient and Stable Electrocatalyst for Hydrogen Evolution Reaction. *J. Am. Chem. Soc.* **2014**, *136*, 4897−4900.

(19) Kong, D.; Wang, H.; Cha, J. J.; Pasta, M.; Koski, K. J.; Yao, J.; Cui, Y. Synthesis of MoS_2 and $MoSe_2$ Films with Vertically Aligned Layers. *Nano Lett.* **2013**, *13*, 1341−1347.

(20) Morales-Guio, C. G.; Stern, L.-A.; Hu, X. Nanostructured Hydrotreating Catalysts for Electrochemical Hydrogen Evolution. *Chem. Soc. Rev.* **2014**, DOI: 10.1039/C3CS60468C.

(21) Xie, J.; Zhang, H.; Li, S.; Wang, R.; Sun, X.; Zhou, M.; Zhou, J.; Lou, X. W. (D.); Xie, Y. Defect-Rich MoS_2 Ultrathin Nanosheets with Additional Active Edge Sites for Enhanced Electrocatalytic Hydrogen Evolution. *Adv. Mater.* **2013**, *25*, 5807−5813.

(22) Merki, D.; Vrubel, H.; Rovelli, L.; Fierro, S.; Hu, X. Fe, Co, and Ni Ions Promote the Catalytic Activity of Amorphous Molybdenum Sulfide Films for Hydrogen Evolution. *Chem. Sci.* **2012**, *3*, 2515−2525.

(23) Chen, Z.; Cummins, D.; Reinecke, B. N.; Clark, E.; Sunkara, M. K.; Jaramillo, T. F. Core−shell MoO_3−MoS_2 Nanowires for Hydrogen Evolution: A Functional Design for Electrocatalytic Materials. *Nano Lett.* **2011**, *11*, 4168−4175.

(24) Hsu, C.-L.; Chang, Y.-H.; Chen, T.-Y.; Tseng, C.-C.; Wei, K.-H.; Li, L.-J. Enhancing the Electrocatalytic Water Splitting Efficiency for Amorphous MoS_x. *Int. J. Hydrogen Energy* **2014**, *39*, 4788−4793.

(25) Smith, A. J.; Chang, Y.-H.; Raidongia, K.; Chen, T.-Y.; Li, L.-J.; Huang, J. Molybdenum Sulfide Supported on Crumpled Graphene Balls for Electrocatalytic Hydrogen Production. *Adv. Energy Mater.* **2014**, DOI: 10.1002/aenm.201400398.

(26) Bian, X.; Zhu, J.; Liao, L.; Scanlon, M.; Ge, P.; Ji, C.; Girault, H. H.; Liu, B. Nanocomposite of MoS2 on Ordered Mesoporous Carbon Nanospheres: A highly Active Catalyst for Electrochemical Hydrogen Evolution. *Electrochem. Commun.* **2012**, *22*, 128−132.

(27) Firmiano, E. G. S.; Cordeiro, M. A. L.; Rabelo, A. C.; Dalmaschio, C. J.; Pinheiro, A. N.; Pereira, E. C.; Leite, E. R. Graphene Oxide as a Highly Selective Substrate to Synthesize a Layered MoS_2 Hybrid Electrocatalyst. *Chem. Commun.* **2012**, *48*, 7687−7689.

(28) Zhao, X.; Zhu, H.; Yang, X. Amorphous Carbon Supported MoS_2 Nanosheets as Effective Catalysts for Electrocatalytic Hydrogen Evolution. *Nanoscale* **2014**, *6*, 10680−10685.

(29) Seger, B.; Laursen, A. B.; Vesborg, P. C. K.; Pedersen, T.; Hansen, O.; Dahl, S.; Chorkendorff, I. Hydrogen Production Using a Molybdenum Sulfide Catalyst on a Titanium-Protected n^+p-Silicon Photocathode. *Angew. Chem., Int. Ed.* **2012**, *51*, 9128−9131.
(30) Greeley, J.; Jaramillo, T. F.; Bonde, J.; Chorkendorff, I.; Norskov, J. K. Computational High-Throughput Screening of Electrocatalytic Materials for Hydrogen Evolution. *Nat. Mater.* **2006**, *5*, 909−913.
(31) Vrubel, H.; Merki, D.; Hu, X. Hydrogen Evolution Catalyzed by MoS_3 and MoS_2 Particles. *Energy Environ. Sci.* **2012**, *5*, 6136−6144.
(32) Karunadasa, H. I.; Montalvo, E.; Sun, Y.; Majda, M.; Long, J. R.; Chang, C. J. A Molecular MoS_2 Edge Site Mimic for Catalytic Hydrogen Generation. *Science* **2012**, *335*, 698−702.
(33) Lukowski, M. A.; Daniel, A. S.; Meng, F.; Forticaux, A.; Li, L.; Jin, S. Enhanced Hydrogen Evolution Catalysis from Chemically Exfoliated Metallic MoS_2 Nanosheets. *J. Am. Chem. Soc.* **2013**, *135*, 10274−10277.
(34) Voiry, D.; Salehi, M.; Silva, R.; Fujita, T.; Chen, M.; Asefa, T.; Shenoy, V. B.; Eda, G.; Chhowalla, M. Conducting MoS_2 Nanosheets as Catalysts for Hydrogen Evolution Reaction. *Nano Lett.* **2013**, *13*, 6222−6227.
(35) Ivanovskaya, A.; Singh, N.; Liu, R.-F.; Kreutzer, H.; Baltrusaitis, J.; Nguyen, T. V.; Metiu, H.; McFarland, E. Transition Metal Sulfide Hydrogen Evolution Catalysts for Hydrobromic Acid Electrolysis. *Langmuir* **2013**, *29*, 480−492.
(36) Huang, X.; Zeng, Z.; Bao, S.; Wang, M.; Qi, X.; Fan, Z.; Zhang, H. Solution-Phase Epitaxial Growth of Noble Metal Nanostructures on Dispersible Single-Layer Molybdenum Disulfide Nanosheets. *Nat. Commun.* **2013**, *4*, 1444−1−8.
(37) Kibsgaard, J.; Chen, Z.; Reinecke, B. N.; Jaramillo, T. F. Engineering the Surface Structure of MoS_2 to Preferentially Expose Active Edge Sites for Electrocatalysis. *Nat. Mater.* **2012**, *11*, 963−969.
(38) Wang, H.; Kong, D.; Johanes, P.; Cha, J. J.; Zheng, G.; Yan, K.; Liu, N.; Cui, Y. $MoSe_2$ and WSe_2 Nanofilms with Vertically Aligned Molecular Layers on Curved and Rough Surfaces. *Nano Lett.* **2013**, *13*, 3426−3433.
(39) Li, Y.; Wang, H.; Xie, L.; Liang, Y.; Hong, G.; Dai, H. MoS_2 Nanoparticles Grown on Graphene: An Advanced Catalyst for the Hydrogen Evolution Reaction. *J. Am. Chem. Soc.* **2011**, *133*, 7296−7299.
(40) Liao, L.; Zhu, J.; Bian, X.; Zhu, L.; Scanlon, M. D.; Girault, H. H.; Liu, B. MoS_2 Formed on Mesoporous Graphene as a Highly Active Catalyst for Hydrogen Evolution. *Adv. Funct. Mater.* **2013**, *23*, 5326−5333.
(41) Ge, P.; Scanlon, M. D.; Peljo, P.; Bian, X.; Vubrel, H.; O'Neill, A.; Coleman, J. N.; Cantoni, M.; Hu, X.; Kontturi, K.; Liu, B. H.; Girault, H. H. Hydrogen Evolution Across Nano-Schottky Junctions at Carbon Supported MoS_2 Catalysts in Biphasic Liquid Systems. *Chem. Commun.* **2012**, *48*, 6484−6486.
(42) Chang, Y.-H.; Lin, C.-T.; Chen, T.-Y.; Hsu, C.-L.; Lee, Y.-H.; Zhang, W.; Wei, K.-H.; Li, L.-J. Highly Efficient Electrocatalytic Hydrogen Production by MoS_x Grown on Graphene-Protected 3D Ni Foams. *Adv. Mater.* **2013**, *25*, 756−760.
(43) Chang, Y.-H.; Wu, F.-Y.; Chen, T.-Y.; Hsu, C.-L.; Chen, C.-H.; Wiryo, F.; Wei, K.-H.; Chiang, C.-Y.; Li, L.-J. Three-Dimensional Molybdenum Sulfide Sponges for Electrocatalytic Water Splitting. *Small* **2014**, *10*, 895−900.
(44) Lee, Y. H.; Zhang, X. Q.; Zhang, W.; Chang, M. T.; Lin, C. T.; Chang, K. D.; Yu, Y. C.; Wang, T. W.; Chang, C. S.; Li, L. J.; Lin, T. W. Synthesis of Large-Area MoS_2 Atomic Layers with Chemical Vapor Deposition. *Adv. Mater.* **2012**, *24*, 2320−2325.
(45) Liu, K. K.; Zhang, W.; Lee, Y. H.; Lin, Y. C.; Chang, M. T.; Su, C. Y.; Chang, C. S.; Li, H.; Shi, Y.; Zhang, H.; Lai, C. S.; Li, L. J. Growth of Large-Area and Highly Crystalline MoS_2 Thin Layers on Insulating Substrates. *Nano Lett.* **2012**, *12*, 1538−1544.
(46) Zhang, W.; Chuu, C.-P.; Huang, J.-K.; Chen, C.-H.; Tsai, M.-L.; Chang, Y.-H.; Liang, C.-T.; Chen, Y.-Z.; Chueh, Y.-L.; He, J.-H.; Chou, M.-Y.; Li, L.-J. Ultrahigh-Gain Photodetectors Based on Atomically Thin Graphene-MoS_2 Heterostructures. *Sci. Rep.* **2014**, *4*, 3826−1−8.
(47) Shi, Y.; Huang, J.-K.; Jin, L.; Hsu, Y.-T.; Yu, S. F.; Li, L.-J.; Yang, H. Y. Selective Decoration of Au Nanoparticles on Monolayer MoS_2 Single Crystals. *Sci. Rep.* **2013**, *3*, 1839−1−7.
(48) Ech-chamikh, E.; Essafti, A.; Ijdiyaou, Y.; Azizan, M. XPS Study of Amorphous Carbon Nitride (a-C:N) Thin Films Deposited by Reactive RF Sputtering. *Sol. Energy. Mater. Sol. Cells* **2006**, *90*, 1420−1423.
(49) Chang, D. W.; Lee, E. K.; Park, E. Y.; Yu, H.; Choi, H.-J.; Jeon, I.-Y.; Sohn, G.-J.; Shin, D.; Park, N.; Oh, J. H.; Dai, L.; Baek, J.-B. Nitrogen-Doped Graphene Nanoplatelets from Simple Solution Edge-Functionalization for N−Type Field-Effect Transistors. *J. Am. Chem. Soc.* **2013**, *135*, 8981−8988.
(50) Wei, D.; Liu, Y.; Wang, Y.; Zhang, H.; Huang, L.; Yu, G. Synthesis of N-Doped Graphene by Chemical Vapor Deposition and Its Electrical Properties. *Nano Lett.* **2009**, *9*, 1752−1758.
(51) Zhang, G.; Sun, S.; Yang, D.; Dodelet, J.-P.; Sacher, E. The Surface Analytical Characterization of Carbon Fibers Functionalized by H_2SO_4/HNO_3 Treatment. *Carbon* **2008**, *46*, 196−205.
(52) Lahaye, J.; Nansé, G.; Bagreev, A.; Strelko, V. Porous Structure and Surface Chemistry of Nitrogen Containing Carbons From Polymers. *Carbon* **1999**, *37*, 585−590.
(53) Sun, Z.; James, D. K.; Tour, J. M. Graphene Chemistry: Synthesis and Manipulation. *J. Phys. Chem. Lett.* **2011**, *2*, 2425−2432.
(54) Jeon, I.-Y.; Yu, D.; Bae, S.-Y.; Choi, H.-J.; Chang, D. W.; Dai, L.; Baek, J.-B. Formation of Large-Area Nitrogen-Doped Graphene Film Prepared From Simple Solution Casting of Edge-Selectively Functionalized Graphite and Its Electrocatalytic Activity. *Chem. Mater.* **2011**, *23*, 3987−3992.
(55) Lin, Z.; Waller, G. H.; Liu, Y.; Liu, M.; Wong, C.-p. 3D Nitrogen-Doped Graphene Prepared by Pyrolysis of Graphene Oxide with Polypyrrole for Electrocatalysis of Oxygen Reduction Reaction. *Nano Energy* **2013**, *2*, 241−248.
(56) Qi, Y.; Mazur, U.; Hipps, K. W. Charge Transfer Induced Chemical Reaction of Tetracyano-p-quinodimethane Adsorbed on Graphene. *RSC Adv.* **2012**, *2*, 10579−10584.
(57) Wang, H. W.; Skeldon, P.; Thompson, G. E. XPS Studies of MoS_2 Formation from Ammonium Tetrathiomolybdate Solutions. *Surf. Coat. Technol.* **1997**, *91*, 200−207.
(58) Weber, Th.; Muijsers, J. C.; van Wolput, J. H. M. C.; Verhagen, C. P. J.; Niemantsverdriet, J. W. Basic Reaction Steps in the Sulfidation of Crystalline MoO_3 to MoS_2, as Studied by X-ray Photoelectron and Infrared Emission Spectroscopy. *J. Phys. Chem.* **1996**, *100*, 14144−14150.
(59) Dupina, J. C.; Gonbeaua, D.; Martin-Litasb, I.; Vinatierb, Ph.; Levasseur, A. Amorphous Oxysulfide Thin Films MO_yS_z (M=W, Mo, Ti) XPS Characterization: Structural and Electronic Peculiarities. *Appl. Surf. Sci.* **2001**, *173*, 140−150.
(60) Martin, I.; Vinatier, P.; Levasseur, A.; Dupin, J. C.; Gonbeau, D. XPS Analysis of the Lithium Intercalation in Amorphous Tungsten Oxysulfide Thin Films. *J. Power Sources* **1999**, *81*−*82*, 306−311.
(61) Freeman, T. L.; Evans, S. D.; Ulman, A. XPS Studies of Self-Assembled Multilayer Films. *Langmuir* **1995**, *11*, 4411−4417.